Available online at www.sciencedirect.com
ScienceDirect
Applied Catalysis B: Environmental 82 (2008) 233–243
APPLIED CATALYSIS B: ENVIRONMENTAL
www.elsevier.com/locate/apcatb

One-pot synthesis of twist-like helix tungsten–nitrogen-codoped titania photocatalysts with highly improved visible light activity in the abatement of phenol

Jingxia Li [a], Jianhua Xu [a], Wei-Lin Dai [a,*], Hexing Li [b], Kangnian Fan [a]

[a] *Department of Chemistry and Shanghai Key Laboratory of Molecular Catalysis and Innovative Materials, Fudan University, Shanghai 200433, PR China*
[b] *Department of Chemistry, Shanghai Normal University, Shanghai 200234, PR China*

Received 11 December 2007; received in revised form 18 January 2008; accepted 26 January 2008
Available online 5 February 2008

Abstract

The twist-like helix W,N-codoped TiO_2 photocatalysts were prepared by a simple one-pot synthesis route to hydrolysis of titania tetrachloride using ammonium tungstate as tungsten and nitrogen sources. The morphology and microstructure characteristics of W,N-codoped titania photocatalysts with different amount of tungsten doping were characterized by means of BET, TEM, SEM, XPS, UV–vis DRS, PLS and XRD. The probable mechanism of codoping effect is proposed. It is presumed that cooperation of nitrogen and tungsten ions leads to produce new states and narrow the band gap between the valence band and conduction band effectively, which will greatly improve the photocatalytic activity in the visible light region. On the other hand, the tungsten ions with changing valences in the W,N-TiO_2 samples are considered to act as trapping sites, which will effectively decrease the recombination rate of photo-induced electrons and holes and then increase the photo-oxidation efficiency of the catalysts. The metal and nonmetal codoped 1%-W,N-TiO_2 sample shows the best photocatalytic activity, which is much superior to P25 under both visible and ultraviolet light irradiation. The superior activity of W,N-TiO_2 photocatalysts can also be ascribed to the special twist-like helix structure with regular holes on the wall, high surface area, large pore volume and well-crystallized anatase phase.

Keywords: Tungsten and nitrogen codoped titania; Mesoporous material; Red shift; Visible light photocatalysis; Phenol abatement

1. Introduction

Nowadays, most interesting application of titanium dioxide is the photocatalytic activity for environment protection since it can decompose a large number of organic and inorganic pollutants [1–5]. However, because of the wide band gap of titanium dioxide, only a small UV fraction of solar light (3–5%) can be utilized. Many researchers paid much attention on ion-doped photocatalysts since modification of TiO_2 with various ions is a powerful way to extend the adsorption light from UV to visible area. Since Sato firstly reported in 1986 that nitrogen doped titanium oxide showed high visible light photocatalytic activities [6], many efforts have been attempted by modification of titanium dioxide with nitrogen and other nonmetals, such as B, C, S, and F, so as to efficiently extend photoresponse from UV to visible light [7–10]. It was commonly reported that the improvement of photocatalysts was attributed to the decrease of the band gap, which is due to the mixture of the states of nonmetals with O_{2p} on the top of the valence band.

Besides that, another key factor affects the wide application of the photocatalyst is its catalytic efficiency, which is controlled by the electron/hole recombination rate, as it controls the availability of photo-excited sites on the catalyst surface [11,12]. It was widely accepted that doping metal ions with changing valence is an optimal method to decrease the recombination rate [13–16]. When anatase TiO_2 is doped with other metal ions with a changing valence, the metal sites are considered to act as trapping sites by accepting the photo-excited electrons from the TiO_2 valence band, and then improve the photo-oxidation activity of the catalysts [12]. Recently, Puddu and co-workers synthesized new WO_3-doped photo-catalysts [11], which showed higher activity with a certain

* Corresponding author. Tel.: +86 21 55664678; fax: +86 21 65642978.
E-mail address: wldai@fudan.edu.cn (W.-L. Dai).

0926-3373/$ – see front matter © 2008 Elsevier B.V. All rights reserved.
doi:10.1016/j.apcatb.2008.01.022

amount of WO_3 doping, due to the enhanced charge separation ability. Gao et al. also prepared series N-doped TiO_2 coupling with WO_3 showing higher activity under both UV and visible light [17], however, there should be further improvement in their works since these preparation processes were too complicated and the TiO_2-N-WO_3 material prepared from immerging TiO_2-N into tungstic acid may result in most of WO_3 adsorbed on TiO_2 surface instead of inserted into the TiO_2 lattice, which may accelerate the photo-electron and holes recombination rate and decrease the photocatalytic activity.

In our previous work, apertured N-doped TiO_2 microtubes had been fabricated by simple hydrolysis of titania tetrachloride using ammonia without any external templates, which showed high visible light response [18]. These hierarchically ordered mesoporous TiO_2 materials may be promising candidates in the field of photocatalysis owing to their large surface area and convenient mass transfer in mesopores in degrading large pollution molecules. Recently, we also used this simple method to prepare twist-like helix N,S-codoped TiO_2 catalysts [19]. During this process, the novel twist-like structured N,S-codoped titania were obtained after hydrolysis of titania tetrachloride using ammonia in the presence of glacial acetic acid and ammonium sulfate. The reaction condition is much milder than that of the conventional methods and the novel twist-like structured N,S-TiO_2 catalyst shows much high activity in both visible and ultraviolet areas. The nitrogen and sulfur doped species play key roles in expanding the photoactivity to visible light region, improving the anatase crystallization and thermal stability. However, the photocatalyst ability to effectively separate photo-induced electron and holes was not further studied. Considering the two major factors affecting the wide application of the photocatalysts, herein we prepared novel metal and nonmetal codoped W,N-TiO_2 catalysts with twist-like helix structure, which was synthesized by the similar simple one-pot method. Although there were some reports concerning W and N-doped titania photocatalyst [11,16,17,20], no hierarchically ordered mesoporous titania with metal and nonmetal codopants has been reported yet. The as-prepared photocatalysts manifest higher photocatalystic activity for photodegradation of phenol under both ultraviolet and visible light irradiation. The factors influencing the photocatalytic activity and the probable mechanism of codoped twist-like helix W,N-TiO_2 are investigated in details.

2. Experimental

2.1. Preparation of mesoporous W,N-codoped titania samples

Titanium tetrachloride ($TiCl_4$, analytical reagent grade) was used as titanium precursor. Commercially available reagents were obtained from Aldrich and used without further purification. The mesoporous W,N-codoped titania samples were prepared by hydrolysis $TiCl_4$ with ammonia in water solution in the presence of glacial acetic acid and ammonium tungstate ($(NH_4)_2WO_4$) as nitrogen and tungsten sources. In a typical procedure, 25 mL of dilute aqueous solution of $TiCl_4$ (3.0 mol L^{-1}) was carefully added into 150 mL deionized water with gentle stirring in ice–water bath to avoid a drastic hydrolysis of $TiCl_4$ in water at room temperature. Subsequently, 4.5 mL of glacial acetic acid and a certain amount of ammonium tungstate were added into the solution, then the mixed solution was quickly cooled down to ambient temperature (about 298 K) by rinsed with running water. After aging in the mother liquor for 24 h, the resultant slurry was suction-filtered and washed with distilled water until pH 7 and then washed carefully with absolute ethanol for three times. The samples were finally obtained after the as-prepared filter residue being vacuum-dried at 353 K for 12 h and calcined at 773 K for 3 h with the ramping rate of 10 K min^{-1}. The W-doping concentration (X) was chosen as 0.5, 1.0, 1.5, 2.0, 3.0, which was the mole percentage of W in the theoretical titania powders. The corresponding concentrations in the as-obtained photocatalysts were denoted as X%-W,N-TiO_2. However, only tungsten doped TiO_2 sample with the unique helix structure cannot be obtained, since ammonia is a very important precipitant and cannot be replaced.

2.2. Characterizations

XRD patterns of W,N-TiO_2 samples (2θ ranges from 20 to 70°) were recorded at room temperature with scanning speed of 2° min^{-1} using Cu Kα radiation (λ = 0.154 nm) from a 40 kV X-ray source (Bruker D8 Advance) and diffracted beam monochromator, operated at 40 mA. The Scherrer equation was applied to estimate the average crystallite sizes of TiO_2 samples: $d = k\lambda/B(2\theta)\cos\theta$, where $B(2\theta)$ is the width of the XRD peak at half peak-height in radian, λ the wavelength of the X-ray in nanometer, θ the angle between the incident and diffracted beams in degree, k is a shape factor of the particle and d is the average crystallite size of the powder sample in nanometer. The content of anatase in TiO_2 powder was calculated as follows: $X_A(\%) = I_A/(I_A + 1.265I_R) \times 100$, where X_A is the content of the anatase phase, I_A and I_R are peak intensities of anatase (1 0 1) and rutile (1 1 0), obtained from X-ray diffraction patterns, respectively.

The textural structures were measured by N_2 adsorption at 77 K in a Micromeritics TriStar ASAP 3000 system, and specific surface areas of W,N-TiO_2 samples were measured using Brunauer–Emmett–Teller (BET) method. The pore size distributions (average pore diameter and mean pore volume) were measured from the N_2 desorption isotherm using the cylindrical pore model (Barrett–Joyner–Halenda (BJH) method). Transmission electron micrographs were obtained using a JEOL 2011 microscope operating at accelerating voltage of 200 kV. The samples for electron microscope investigation were prepared by dispersing the powder in ethanol and applying a drop of very dilute suspension on copper grids. The suspensions were dried by slow evaporation at ambient temperature. Scanning electron micrographs were obtained using Philips XL 30 electron microscope. The samples were deposited on a sample holder with a piece of adhesive carbon tape and were then sputtered with a thin film of gold.

Simultaneous thermal gravimetric (TG) and differential thermal analysis (DTA) measurements were performed between room temperature and 1023 K on a PerkinElmer 7 series thermal analyzer, using Al_2O_3 as a reference. Samples were heated at a rate of 10 K min^{-1} under a dynamic dry air atmosphere of 50 mL min^{-1}. For each experiment, 10–15 mg of sample was used. X-ray photoelectron spectroscopy (XPS) measurements were performed on a PHI 5000C ESCA System with Mg Kα source at 14.0 kV and 25 mA. All the binding energies were referenced to the C_{1s} peak at 284.6 eV of the surface adventitious carbon. All samples were calcined under 723 K for 3 h to eliminate removable tungsten and nitrogen adsorbent. Ar^+ etching experiments were carried out by using a PHI Ar-ion gun with a current of 6 mA and an acceleration voltage of 2.0 kV (ion current, 8 μA), which gives a sputtering rate of ca. 33 Å/min. After sputtering for 3 min, the elemental composition of the freshly etched surface is determined. UV–visible diffuse reflectance spectra (UV–vis DRS) were achieved using a UV–visible spectrophotometer (Shimadzu UV-2450) using $BaSO_4$ as the reference sample.

2.3. Adsorption and degradation of phenol

The photocatalytic activity experiments of the W,N-TiO_2 series and Degussa P25 for the decomposition of phenol in ultraviolet and visible light irradiation were performed in a self-constructed quartz photoreactor which consists of a quartz tube (diameter 20 mm, length 250 mm) placed in the middle of the lamp bracket. Four 8 W lamps with various wavelengths (243, 365 or 420 nm) were used as ultraviolet and visible light source. In each experiment, 0.050 g catalyst was placed into 50 mL of reactant solution with the initial concentration of 0.060 g L^{-1} (for ultraviolet experiment) or 0.030 g L^{-1} (for visible light experiment) of phenol. The reaction solution was sonicated for 20 min with a sonicator to obtain a homogeneous suspension. The reactant was adsorbed on the catalyst surface without irradiation for about 60 min to achieve the adsorption/desorption equilibrium established. The temperature was controlled at 298 ± 1 K during the overall decomposition process. During all experiments, the photoreactor was continuously purged with air at a flow rate of 100 mL min^{-1} to guarantee sufficient O_2 concentration in the reaction medium. After saturation of adsorption into catalysts, 3 mL of the prepared suspension was taken as a blank probe before irradiation and, after filtration of the catalyst with a dialyzer with the pore of 2 μm, for the UV–vis analysis. After that, the quartz tube was put into the photoreactor and the lamps were switched on to start the process of degradation. In every 0.5 h, several milliliters of solution were sampled from the reaction mixture through a membrane filter in order to measure the reactant concentration in the same way as the blank probe, while the sampling interval was 1 h for visible light photodegradation. The concentration of phenol was calculated from the height of peak at 270 nm in UV–vis spectra (Shimadzu, UV-2450) by using the calibration curve. The measurements were repeated for each catalyst and the experimental error was found to be within ±3%.

3. Results and discussion

3.1. X-ray diffraction

The phase structure, crystallite size and crystallinity of TiO_2 play important roles in photocatalytic activity and many studies have confirmed that anatase phase of titania shows higher photocatalytic activity than brookite or rutile phase [21]. XRD was used to investigate the changes of phase structure of TiO_2 samples prepared with different ammonium tungstate addition. In Fig. 1, the XRD patterns of W,N-TiO_2 with different W-doping concentration calcinated at 773 K for 3 h are provided. The major crystalline phase detected in all samples is anatase. As seen in Fig. 1, if compared to the pure TiO_2, the peak width and the intensity of anatase phase at $2\theta = 25.3^\circ$ in all the W,N-codoped TiO_2 catalysts are much stronger and sharper, indicating the higher crystallinity of anatase phase than the pure TiO_2. It is worth noting that no WO_3 phase could be observed in all the XRD patterns, even the doping amount reaches 3%. Thus we can propose that all the tungsten ions may be incorporated into the titania lattice and replaced titanium ions to form W–O–Ti bonds or located at interstitial sites. The average size of crystallites was estimated based on the broadening of (1 0 1) peak at $2\theta = 25.3^\circ$ using the Scherrer equation [22], $d = k\lambda/B(2\theta)\cos\theta$, where k is a shape factor of the particle (it equals to 1 if a spherical shape is assumed), λ and θ the wavelength and the incident angle of the X-rays, and B the full width half maximum (FWHM) of the 2θ peak, respectively. Structure analysis of the W,N-TiO_2 with different tungsten doping contents suggests that the anatase phase and the particle size of all the as-prepared TiO_2 catalysts are about 10–11 nm, as shown in Table 1, which are much smaller than that of P25 with a size of 21 nm. The small crystallite size indicates that the preparation method used in the present work can effectively prompt the crystallization and inhibit the grain growth when compared with P25. Furthermore, the crystallite size of the

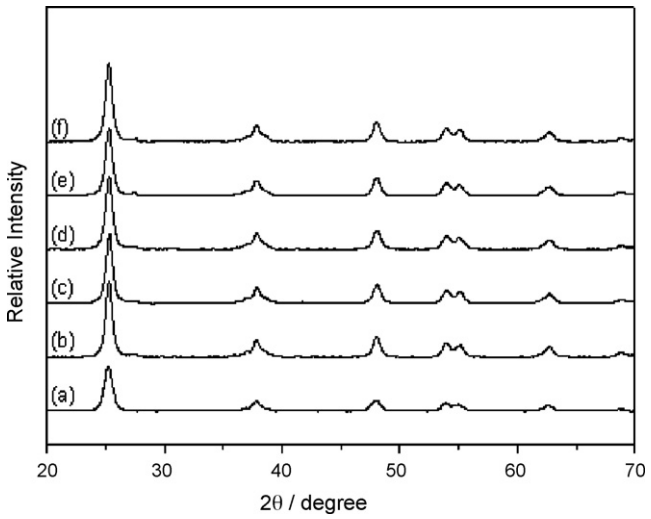

Fig. 1. X-ray diffraction patterns of X%-W,N-TiO_2 with different W-doping concentration: (a) TiO_2; (b) 0.5%-W,N-TiO_2; (c) 1%-W,N-TiO_2; (d) 1.5%-W,N-TiO_2; (e) 2%-W,N-TiO_2; (f) 3%-W,N-TiO_2.

Table 1
Textural and structural properties of W,N-TiO_2 samples with different W-doping concentration

Sample	Surface area[a] ($m^2\ g^{-1}$)	Pore volume[a] ($cm^3\ g^{-1}$)	Average pore diameter (nm)	Crystallite phase[b] (%)	Crystallite size[c] (nm)
TiO_2	81	0.19	7.4	A: 100	A: 9.9
0.5%-W,N-TiO_2	78	0.18	7.3	A: 100	A: 11
1%-W,N-TiO_2	80	0.20	6.2	A: 100	A: 11
1.5%-W,N-TiO_2	82	0.19	6.1	A: 100	A: 11
2%-W,N-TiO_2	80	0.18	6.1	A: 100	A: 11
3%-W,N-TiO_2	79	0.18	6.1	A: 100	A: 11
P25	51	0.16	16.0	A: 77, R: 23	A: 21; R: 24

[a] BET surface area, average pore volume of the W,N-TiO_2 samples estimated from nitrogen adsorption.
[b] Ratio of phase of titania based on XRD data, where A and R represent the anatase and rutile phases, respectively.
[c] Average size of titania crystallites estimated from Scherrer equation.

samples after nitrogen and tungsten doping changed slightly, illustrating that the nitrogen and tungsten did not change the catalysts structure and retained the well anatase crystallization after the doping process.

3.2. Particle morphology

The morphology of the twist-like helix pure TiO_2 and 1%-W,N-TiO_2 catalysts was investigated with SEM and TEM, as shown in Fig. 2. The SEM image of the pure TiO_2 anatase sample calcinated at 773 K was also shown in Fig. 2a. It is worth to note that the TiO_2 samples kept its twist-like helix structure and maintained the three-dimensional helix nature of particles after high temperature calcination, with the average holes about 1 μm × 3 μm. The shape of these samples are almost unchanged after W,N-doping process as shown in Fig. 2b. High-resolution SEM image shown in Fig. 2 suggests that the average screw-pitch of each twist in all the catalyst is about 50–100 μm, the array of ventages exhibited regularly between conterminous twists, and the average diameter of each hole is about 1 μm × 3 μm with the interval of ca. 4 μm. The size of twist-like TiO_2 sample was comparatively uniformly sized. TEM analyses were also performed to examine the nanocrystallites that make up the twist-like helix W,N-TiO_2 samples. Fig. 2d presents the nanocrystalline nature of anatase TiO_2. It is found that the size of anatase nanocrystallites is approximately 11 nm, which is consistent well with that calculated from the XRD data (see Fig. 1). High-resolution TEM confirmed that the samples were comprised of connected crystalline titania nanoparticles, with a lattice spacing consistent with the anatase phase (0.352 nm), which fit well with the results from XRD patterns. Such anatase crystallinity

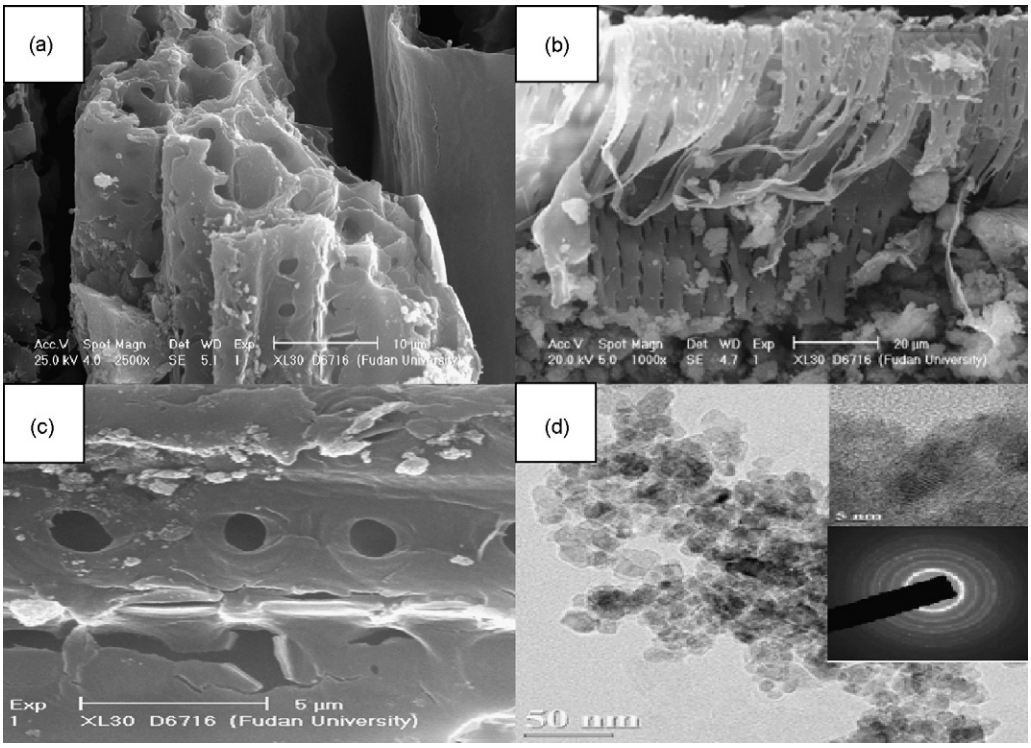

Fig. 2. SEM images of W,N-TiO_2 samples: (a) TiO_2; (b) 1%-W,N-TiO_2; (c) enlarged SEM images of W,N-TiO_2; (d) the TEM images of W,N-TiO_2-AS. The SAED image in inset (d) displaying the crystalline nature (anatase) of the titania nanoparticles.

in the mesoporous TiO_2 is highly desirable in photocatalysis [23]. The electron diffraction measurement of the selected area (Fig. 2d, inset) demonstrated clear diffraction lines representative of anatase, namely (1 0 1), (2 0 0), (0 0 4) and (2 1 1), further indicating that the sample was in well-crystallized anatase phase and it was also confirmed by the result of X-ray diffraction.

The formation of hierarchical porous shapes was usually explained by the facet selectivity of the templates during the crystallite growth of the synthesis, while no template is used in our present work for the synthesis process, and the twist-like helix morphology was formed during the process. There might be another mechanism for the formation of TiO_2 helix. We find that the use of acetic acid as a dispersing agent is of crucial importance in the preparation of apertured titania microtube structure. The essential role of acetic acid in promoting the formation of mesoporous TiO_2 microtubes may be understood by taking into account from the following two aspects. Firstly, adequate amount of acetic acid may behave as a ligand due to acetate anion, which was similar with those studies on the chemical modification of alkoxides with organic agents before hydrolysis. Similar results were also observed by Livage et al. [24] and Doeuff et al. [25] using acetate anions as ligands to prepare TiO_2 monolithic gel. In the present work, the bidentate acetate ligands may also replace Cl^- in $TiCl_4$ precursor and be bounded to metal ions, which will modify the polymeric structure at a molecular level, thus will promote the emergence of 3D-type polymeric structures. The formed three-dimensional network polymers will transfer to helix like structure with regular ventages during further decomposition of acetate ligands in the gel at programmed heating process. Secondly, acetic acid apparently acts not only as ligands, but also affects the rate of gelation. It will inhibit the hydrolysis–condensation reaction, which will prolong the gelation time and prevent forming irregular TiO_2 particles as synthesized by normal rapidly hydrolysis process [26]. As we are known, in most systems, the hydrolysis and condensation process rapidly proceeds when $TiCl_4$ are employed as precursor. The prolonged gelation time will stabilize the net structure of sol precursor, thereby the stability of these 3D-type structure was improved. Hence the twist-like helix structure was also observed after heated at 723 K for 3 h.

3.3. The specific surface area, pore size and pore volume

Since it is widely accepted that heterogeneous photocatalyst is influenced by the surface area and pore structure, we carefully investigated the effects of tungsten doping amount on the pore structure and BET surface area of twist-like helix TiO_2 samples based on nitrogen adsorption and desorption measurements. Table 1 lists the physicochemical properties of W,N-TiO_2 series with different W-doping concentration. The pure TiO_2 sample shows a specific surface area of 81 $m^2\ g^{-1}$, which is much larger than Degussa P25. After the doping of nitrogen and tungsten to the catalysts, the specific pore volume and pore diameter changed slightly, however, the BET surface area maintained a certain value, suggesting a little influence of the WO_3 doping amount on the specific surface area of TiO_2 microstructures. Although there is still much debating on whether activity of a photocatalyst can be related to the catalyst surface area, since photocatalytic reactions are believed to proceed only on the illuminated surface. However, one could argue that adsorption on the catalyst surface would at least help to ''concentrate'' the reactant molecules for the photoreactions and the photons might be scattered between the nano-sized TiO_2 particles. Also, photogenerated electrons and vacancies as well as the adsorbed molecules might be able to diffuse more or less at the catalyst surface, causing the photoreactions more easily to happen [27]. The high specific surface area of pure TiO_2 and W,N-TiO_2 samples with twist-like helix structure may help this process more efficiently in the photodegradation. Hence the series of W,N-codoped catalysts show higher photoactivity than P25 in the decomposition of aqueous phenol solution.

Fig. 3 shows the nitrogen adsorption/desorption isotherm of pure W,N-TiO_2 sample, which indicates a type IV-like isotherm with an inflection of nitrogen-adsorbed volume at $P/P_0 = 0.70$ (type IV isotherms with H_2 hysteresis loops), indicating the presence of well-developed mesoporosity in the twist-like helix titania samples. Moreover, the inset in Fig. 3 shows the pore size distribution plots calculated using the Barrett–Joyner–Halenda equation from the adsorption branch of the isotherm. The pore size distribution measurement indicates that the twist-like helix W,N-codoped titania sample has pronounced mesoporosity of a narrow pore size distribution with an average pore diameter at ca. 6.5 nm. These results illustrate that doping with W or N species does not significantly change the textural properties of TiO_2. The dopants embedded in the TiO_2 network of the mesoporous pore walls, and the pore channels remain open. Such stable mesoporous structure after 733 K calcination, open mesoporous architecture, large surface area and 3D-connected pore system all play an important role in catalyst design for its ability to improve the molecular transport of reactants and products [28]. It is known that commercial Degussa P25 shows no mesoporosity, which might be one

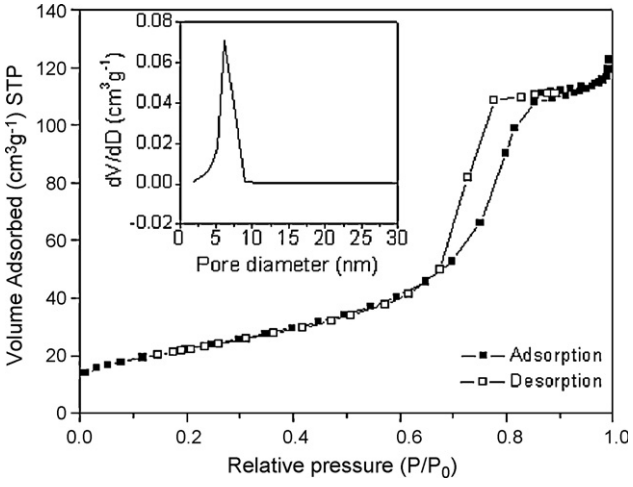

Fig. 3. Nitrogen adsorption/desorption isotherms and the corresponding pore size distribution (inset) of 1%-W,N-TiO_2.

reason why the present W,N-TiO_2 sample shows much higher photoactivity than P25.

3.4. XPS analysis

To investigate the chemical states and the concentrations of nitrogen and tungsten atoms incorporated into the W,N-TiO_2 photocatalysts, all the samples were analyzed by XPS. The nitrogen and tungsten elements could be chemically adsorbed on the TiO_2 surface or doped into TiO_2 lattice, and the adsorbed elements could be eliminated by thermal treatment. The characterization was performed after calcinated at 723 K for 3 h to eliminate the simply adsorbed N or W species and to prove the doping of them.

Fig. 4a shows the XPS spectra of the 1%-W,N-TiO_2 catalyst with the information of binding energies and intensities of the surface elements. The relative quantities of the outermost surface compounds of W,N-TiO_2 catalysts with different tungsten doping were calculated in Table 2. The concentration of doped W atoms increased with the increase of added ammonium tungstate content, while the nitrogen doped content maintained a certain value. At present, nitrogen contents in all the N-doped catalysts are not same when using various methods and different nitrogen precursors. In our present work, ammonia was used as precipitant to prepare twist-like helix TiO_2 samples, so 0.4% nitrogen species in TiO_2 sample came from the ammonia precipitant. However, W,N-TiO_2 catalysts with different nitrogen and tungsten contents were prepared using ammonium tungstate as nitrogen and tungsten sources. Considering that ammonia was also used as precipitant in this process, addition of small amount of ammonium tungstate may be not enough to improve the nitrogen content in 0.5%-W,N-TiO_2 sample and the 0.4% nitrogen dopant may also be considered to come from ammonia. However, with the increasing amount of ammonium tungstate, the maximum nitrogen content will be obtained as high as 0.6% in 2.0%-W,N-TiO_2 sample. A small amount of carbon element is ascribed to the adventitious hydrocarbons from the circumstance or the XPS instrument itself. To date, the assignment of the XPS peak of N_{1s} has still been under debate. In many cases, the peak at about 399 eV is attributed to substitutional nitrogen doping [29,30]. As shown in Fig. 4b, most nitrogen species in W,N-TiO_2 catalysts are located at 399.5 eV, which confirmed the formation of N–Ti–O bonds or the interstitial nitrogen bound to one lattice oxygen and formed a N–O species. Both the substitutional and interstitial nitrogen species could affect the electronic bond structure of TiO_2 and improve the photocatalytic activity in the visible light region.

From the Ti_{2p} XPS spectra of all the TiO_2 catalysts after calcination at 773 K, it can be observed that for all of the XPS signals $Ti_{2P3/2}$ can be fitted into two components, one located at 458.0 eV, attributed to Ti(III) species, and the other located at 458.9 eV, assigned to Ti(IV) species, as shown in Fig. 4c [31,32]. This result indicates that there are two types of titanium oxide species on the surface of the twist-like helix W,N-codoped titania, and the relative amounts of the Ti(III) and

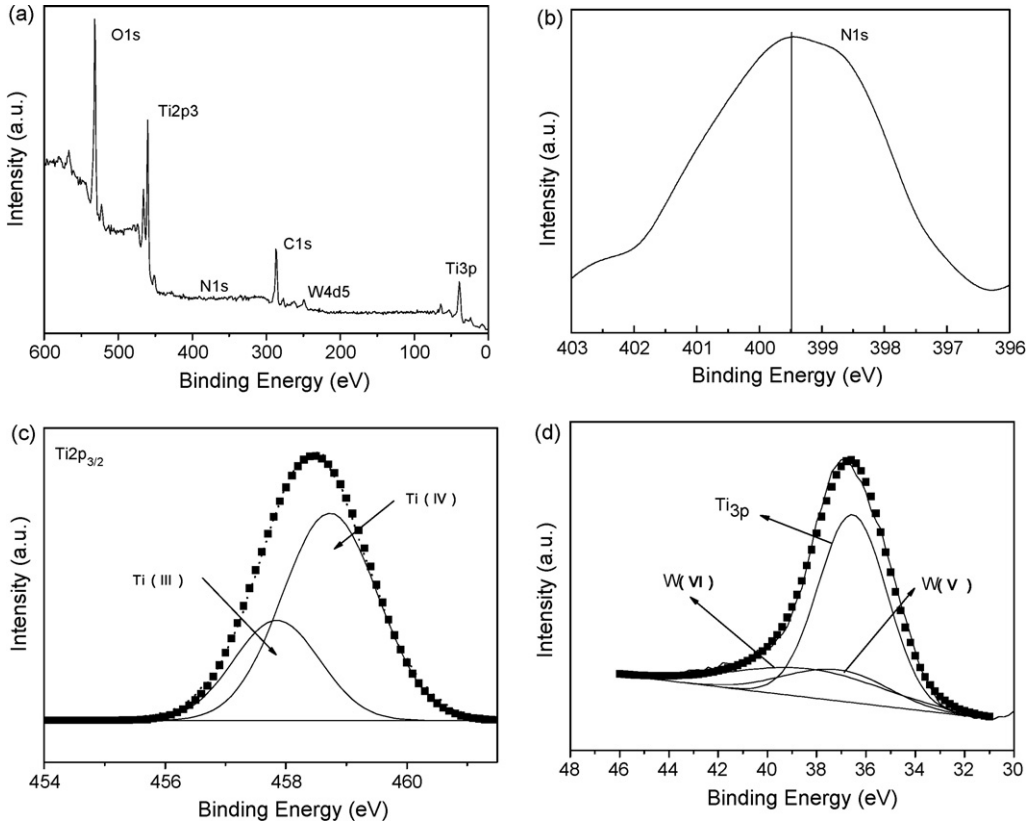

Fig. 4. (a) Full XPS regions for the 1%-W,N-TiO_2; (b) Ti_{2p} of W,N-TiO_2 catalysts with different tungsten doping; (c) peak-fitting XPS spectrum of Ti_{2p} of the 1%-W,N-TiO_2; (d) peak-fitting XPS spectrum of W_{4f} of the 1%-W,N-TiO_2.

Table 2
Proportion of the surface species of TiO_2 and various *X*%-W,N-TiO_2 samples

Sample	W[a] (mol%)	N[b] (mol%)	Ti[c] (mol%)	O[d] (mol%)	Ti^{3+}/Ti^{4+e}	W^{5+}/W^{6+e}
TiO_2	0	0.4(0.4)	28.0	71.6	0.15	0
0.5%W,N-TiO_2	0.5(0.5)	0.4(0.4)	25.7	72.4	0.16	0.31
1.0%W,N-TiO_2	0.8(0.8)	0.5(0.5)	26.1	72.6	0.19	0.32
2.0%W,N-TiO_2	1.7(1.2)	0.6(0.5)	25.6	72.1	0.20	0.39
3.0%W,N-TiO_2	1.8(1.4)	0.6(0.5)	24.9	72.7	0.22	0.40

(a, b, c, d) Calculated according to the peak areas of W_{4d}, N_{1s}, Ti_{2p} and O_{1s}, respectively.
[e] Calculated according to the curve-fitting results of the $Ti_{2p3/2}$ and W_{4f} XPS spectra of catalysts; data in (): after Ar^+ etching for 3 min (~10 nm depth).

Ti(IV) species are shown in Table 2. Compare to pure TiO_2, W,N-codoped TiO_2 show higher molar ratio of Ti(III) to Ti(IV) species, and the concentration of Ti(III) enhanced with the increase of tungsten doping content, suggesting the strong interaction formed between titanium and tungsten species. Since titanium (III) oxide is a narrow band gap semiconductor and its energy level is located between the valence band and the conduction band of TiO_2 [33,34], the electrons in the new valence band may be excited to the conduction band of TiO_2. Therefore, the higher concentration of Ti(III) in the W,N-TiO_2 sample than that in the pure TiO_2 partially contributed to the higher photocatalytic activity of the W,N-TiO_2 catalysts.

In the present work, two energy levels of tungsten were measured in the W_{4d} and W_{4f} regions. However, the W_{4d} peak is broad and cannot be used to determine the oxidation state of tungsten, so we analyzed the W_{4f} region as shown in Fig. 4d. With the increasing tungsten oxide loading, the intensity of the W_{4f} XPS peaks also increases. The measured spectra appear similar for all samples and show identical positions for the W_{4f} peaks except for N-TiO_2 sample. Although analysis of the W_{4f} region is complicated by interference from the Ti_{3p} level of the TiO_2, we still can clearly see that the $W_{4f7/2}$ peak of 1%-W,N-TiO_2 shifts to a higher level of binding energy when compared with that of WO_3, as shown in Fig. 4d. The shift of W_{4f} peaks to a higher binding energy indicates lower electron density of the tungsten atom in the W,N-TiO_2 sample, and further suggests the formation of W–O–Ti bonds. The formation of W–O–Ti bonds and the N–Ti–O bonds can enhance the crystallization degree of anatase phase during calcination process and most importantly increase the visible light adsorption ability [35].

By the curve-fitting procedure based on the theory of Doniach and Sunjic [36,37], it is possible to determine the valence of tungsten from the position of the W_{4f} level. Both W(VI) and W(V) species at $W_{4f7/2}$ (of 35.2 and 34.2 eV [38]) for the W_{4f} spin–orbit components have been detected. As shown in Table 2, with the increase of tungsten doping, the mole ratio of W(V) to W(VI) increased at first. The increased formation of W(V) can be understood from following considerations. When TiO_2 doping with tungsten species, W^{6+} (average ion radius = 62 pm) species will replace the Ti^{4+} (average ion radius = 62 pm) to form W–O–Ti bond as above proved and then the photo-induced electrons will effectively be trapped by nearby W^{6+} species, hence generating W(V) through $W^{6+} + e = W^{5+}$ process. So the existence of W(V) species further indirectly demonstrated the formation of the W–O–Ti bond. Nevertheless, too much tungsten doping content did not further improve the W^{5+} concentration as shown in Table 2, since not all of the doping tungsten species can replace the Ti^{4+} and part of them will deposit on the surface of TiO_2 catalyst. The deposited WO_3 on the surface will act as recombining sites of electrons and holes which is undesirable to the photocatalytic reactions. These results can well explain the highest activity of 1%-W,N-TiO_2 compared with other W,N-TiO_2 catalysts, since certain amount of tungsten doping is favored to separate photo-induced electron and holes effectively and then to increase the photocatalytic ability of W,N-TiO_2 catalysts.

The depth analysis result of tungsten and nitrogen atoms in the lattice analyzed by XPS with Ar^+ etching technique was also shown in Table 2, and it is found that similar amount of tungsten and nitrogen species exists regardless of the 3 min Ar^+ etching (~10 nm depth) for low doping W,N-TiO_2 samples. As seen from Table 2, higher tungsten contents resulted in the enrichment of tungsten atoms on the surface, which is in well consistence with the results from PL UV–vis DRS spectra, showing that the higher deposited tungsten oxide inhibited the adsorption of visible light. However, although there are some deviations in the data for the nitrogen contents after Ar^+ etching compared with those un-etched ones, most of the doped nitrogen contents are similar, considering the errors for the quantitative XPS, indicating that the surface nitrogen and tungsten contents of the W,N-TiO_2 catalyst is uniform in the present work.

3.5. PLS and DRS analysis

To further prove that the W,N-TiO_2 catalysts can efficiently inhibit the recombination of excited electrons and holes and then produce more active sites, the photoluminescence spectra (PLS) was recorded. Photoluminescence emission has been widely used to investigate the efficiency of charge carrier trapping, migration, and transfer and to understand the fate of electron/hole pairs in semiconductor particles since PL emission results from the recombination of free carriers [39–41]. Fig. 5 demonstrated that both TiO_2 and 1%-W,N-TiO_2 samples exhibited two PLS peaks. The signal at about 382 nm could be attributed to an emission peak from band edge free excitation. The higher intensity of W,N-TiO_2 mainly corresponded to the more oxygen vacancies and/or defects in the catalysts than that of pure TiO_2 [42]. While the peak appeared at 560 nm is emission signals originating from the charge-transfer transition of an oxygen vacancy trapped electron. Because the PL emission is the result of the recombination of excited

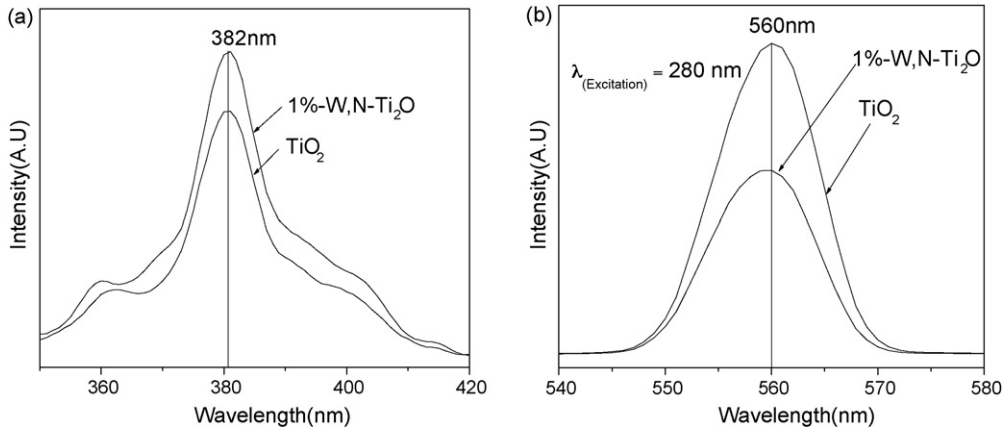

Fig. 5. PLS spectra of TiO_2 (a) and 1%-W,N-TiO_2; (b) catalysts.

electrons and holes, the lower PL intensity at 560 nm of the doped sample indicates a lower recombination rate. As shown in Fig. 5, the W,N-doping TiO_2 leads to a lower intensity of peak located at 560 nm. Therefore, it can be deduced that the recombination efficiency of the tungsten doped titania is relatively slower in the ultraviolet and visible light irradiation, which is probably the reason of the increase of photocatalytic activity of W,N-TiO_2 than that of pure TiO_2.

From Fig. 5, we can get the conclusion that more electrons can transfer from the valence band to the conduction band and the charge separation efficiency of the photo-induced electrons and holes enhanced in the W,N-TiO_2. The effective inhibition of the recombination can be attributed to the two following pathways: the doped tungsten species with changing valence can trap the electrons through $W^{6+} + e = W^{5+}$ process as previous proved. This process will effectively separate the photo-induced holes and electrons. The other way is the existence of the titanium (III) oxide and the W,N-codoping into the TiO_2 structure will form a new band located just above the conduction band of TiO_2 as XPS proved. The excited electrons can transfer from the valence band to the new levels, which can also decrease the photo-induced electrons and holes recombination rate.

Furthermore, the higher photoactivity of W,N-TiO_2 can also be attributed to the higher visible light absorbance, which can be easily proved by DRS spectra. The UV–vis DRS spectra of the mesoporous *X*%-W,N-TiO_2 samples are shown in Fig. 6. W,N-TiO_2 sample with 0.5% WO_3 doping concentration exhibits higher red shift compared with the other W,N-TiO_2 catalysts, and following the 1.0%-W,N-TiO_2 one. However, all of the optical band edge of mesoporous W,N-TiO_2 samples exhibit a remarkable red shift with respect to that of pure TiO_2 and P25. Band gap calculation of W and N codoped TiO_2 catalysts are shown in Table 3. The adsorption edge of W,N-TiO_2 samples shifted greatly toward a higher wavelength (>400 nm) compared to that of P25 (~396 nm) and pure TiO_2. The band gap of these samples calculated by the absorption edge are estimated to be 2.90–2.96 eV, which is not only much lower than P25 (~3.15 eV), but also is smaller than 3.2–3.3 eV for the nondoped anatase. Considering that the band gap of TiO_2 (~2.95 eV) with 0.4% nitrogen doping content is more lower than P25 as shown in Table 3, the observation of optical bands in the visible range (400–550 nm) can be partly contributed to N dopants. The formation of N–Ti–O bands as proved by XPS spectra will create an N-induced midgap level, as same as other researchers proved, and then to improve the catalysts' activity effectively in visible light regions. Also from Table 3, effects of tungsten atoms on visible light absorption can be directly observed in absorption experiments since 0.5%-W,N-TiO_2 shows higher absorption edge (~430 nm) and lower band gap (~2.88 eV) than TiO_2 (420 nm, 2.95 eV), although all the samples show similar nitrogen contents. It has been proved that tungsten species in the W,N-TiO_2 samples will also affect the visible absorption since tungsten has been shown to promote the creation of surface oxygen vacancies, to enhance the surface acidity, and to form W–Ti–O bands, which proved to help the formation of a greater number of Ti^{3+} sites as XPS and PLS spectra proved. It is possible that the optical properties of the calcined material can also be attributed to Ti^{3+} species and oxygen vacancies, as these results have been reported to have transitions between 3.20 and 2.32 eV and are located above the valence band edge.

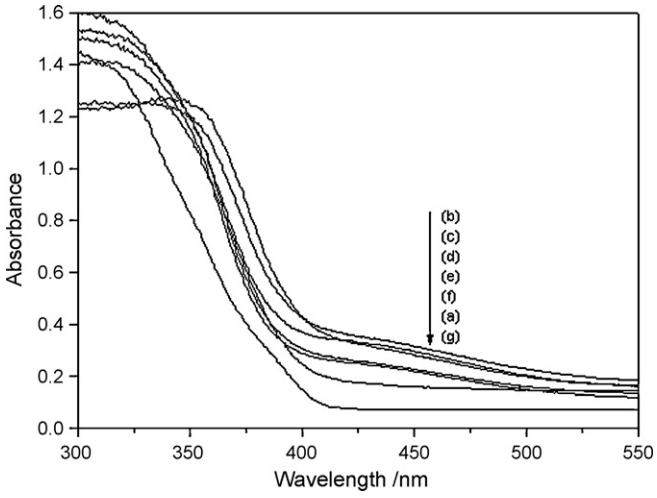

Fig. 6. UV–visible diffuse reflectance spectra of (a) TiO_2; (b) 0.5%-W,N-TiO_2; (c) 1%-W,N-TiO_2; (d) 1.5%-W,N-TiO_2; (e) 2%-W,N-TiO_2; (f) 3%-W,N-TiO_2; (g) Degussa P25.

Table 3
Nitrogen and tungsten content, photoabsorption threshold value and band gap energies of different catalysts

Sample	N (mol%)	W (mol%)	Absorption edge (nm)	Band gap[a] (eV)
TiO_2	0.4	0	420	2.95
0.5%-W,N-TiO_2	0.4	0.5	430	2.88
1%-W,N-TiO_2	0.5	0.8	425	2.92
2%-W,N-TiO_2	0.6	1.7	423	2.93
3%-W,N-TiO_2	0.6	1.8	420	2.95
P25	0	0	396	3.15

[a] Calculated from the absorption edge.

However, further increased tungsten contents resulted in slightly blue shift of the absorption edge from 430 to 420 nm, and the band gap from 2.88 to 2.95 eV, which can be considered to come from the higher tungsten contents deposited on the catalysts' surface and the inhibition of the adsorption of visible light at some extent. Thus, we can make the conclusion that codoped certain amount of tungsten and nitrogen species will cooperatively induce the band gap energy and improve the activity under visible light irradiation. The light absorbance of the W,N-TiO_2 in the visible light region is of great importance for its practical application since it could be activated even by sunlight.

3.6. Photocatalytic activity of TiO_2 samples in photodegradation of phenol

To evaluate and to compare the photocatalytic activity of the mesoporous W,N-TiO_2 samples, the degradation reactions of aqueous solution of phenol were performed as photoreaction probes under UV and visible irradiation. The course of phenol photodecomposition using the catalyst *X*%-W,N-TiO_2 was given in Figs. 7 and 8, and Degussa P25 was used as the reference sample for comparison purpose. In the controlled experiment in which phenol is in TiO_2 suspensions in the dark

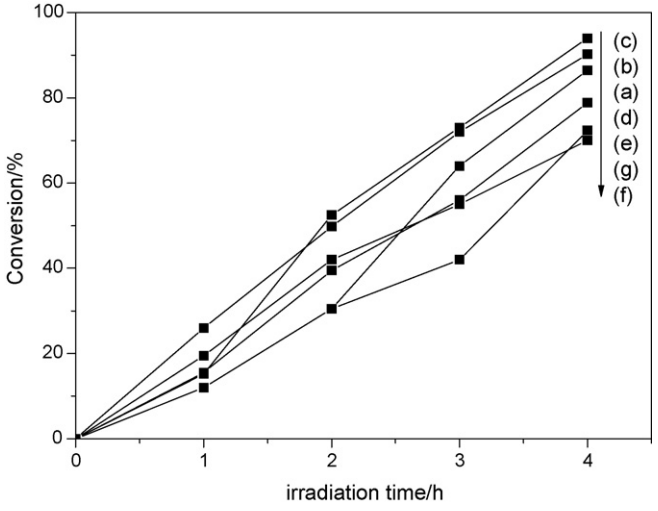

Fig. 7. Time courses of the photocatalytic decomposition of phenol on (a) TiO_2; (b) 0.5%-W,N-TiO_2; (c) 1%-W,N-TiO_2; (d) 1.5%-W,N-TiO_2; (e) 2%-W,N-TiO_2; (f) 3%-W,N-TiO_2; (g) Degussa P25.

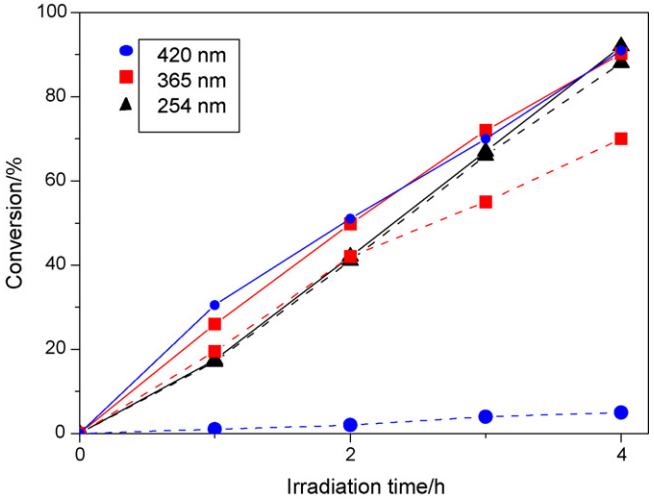

Fig. 8. Time courses of the photocatalytic decomposition of phenol on 1%-W,N-TiO_2 samples (straight line) and Degussa P25 (dash line) under 254 nm; 360 nm; 420 nm lights, respectively.

or is illuminated with ultraviolet light in the absence of TiO_2 does not exhibit photocatalytic activity.

As shown in Fig. 7, most of the samples demonstrated considerably high photoactivity under UV irradiation. It was found that the 1%-W,N-TiO_2 sample exhibited the best photocatalytic efficiency in degradation of phenol in all tested TiO_2 samples and phenol was almost completely eliminated within 4 h. It is evident that the photoactivity of the samples with twist-like helix structure is superior to the standard photocatalyst Degussa P25. The higher photocatalytic activity of the 1%-W,N-TiO_2 sample is partially due to its high specific surface area, special helix structure and mesoporous pores, small crystallite size and good anatase crystallization. Except that, as we know, when anatase TiO_2 is doped with tungsten species with changing valence, improved charge separation can result from doping the tungsten ions as PLS spectra illustrated. Moreover, the higher acidity of WO_3 than TiO_2 can modify the affinity of substrates for the catalyst surface and the adsorption equilibrium of the catalyst. When the addition value of WO_3 was higher than 1%, too much WO_3 deposited on the catalysts surface will act as trapping site by accepting the photo-excited electrons from the TiO_2 valence band, hence the photo-induced electrons and the photocatalytic activity decreased [11]. Consequently, we considered that the tungsten doping concentration had an optimal value.

Considering the sunlight is composed of different wavelength from ultraviolet to visible light, we continue the investigation of catalytic activity with irradiation wavelength at 254, 365 and 420 nm. With the irradiation wavenumber transferred from ultraviolet to visible region, both 1%-W,N-TiO_2 and P25 showed decreased activity as seen in Fig. 8. However, the photoactivity decrease of 1%-W,N-TiO_2 was slight and could not be obviously detected while the P25 had nearly no activity at all in the visible light region (420 nm). The expanded photoactivity under visible light is due to the tungsten and nitrogen codoping according to the common accepted opinions, since the formation of N–Ti–O bonds will form a new

energy band, which will induce the narrowing of the band gap of TiO_2 very much. Also the formation of Ti(III) oxide and oxygen vacancies as XPS spectra proved will contribute to narrow the band gap and to increase the photoactivity of W,N-codoping TiO_2 under visible light irradiation. The excellent photocatalytic activity of the W,N-TiO_2 sample could also be attributed to the well-crystalline anatase phase which facilitates the transfer of photo-induced vacancies from bulk to surface for degradation of organic compounds. The photocatalytic performance is also related to the mesoporous microstructure of the W,N-TiO_2 samples with large BET surface areas and a 3D-connected pore system which can help to concentrate the reactant molecules for the photoreactions and the photons might be scattered between the nano-sized TiO_2 particles.

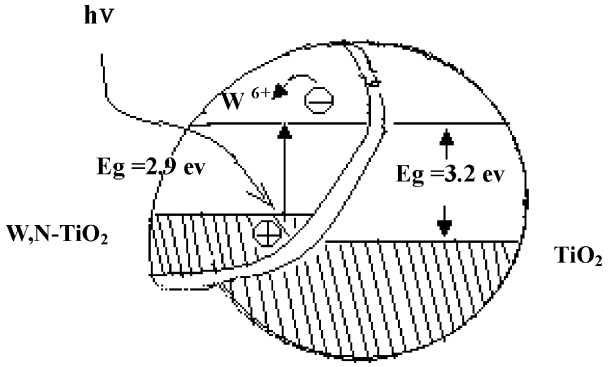

Scheme 1. Diagram of the photocatalytic mechanism of W,N-codopted TiO_2 and pure TiO_2.

3.7. Discussion

Taking into account the codoped W,N-TiO_2 showed high activity under both visible and ultraviolet lights, the probable schematic diagram is proposed. On the one hand, the nitrogen and tungsten codopants can narrow the band gap of TiO_2 from 3.2 to 2.9 eV. Sato et al. firstly reported that the nitrogen doping will enhance the photocatalytic activity effectively due to mixing the nitrogen 2p with oxygen 2p states on the top of the valence band. In our present work, the existence of N–Ti–O bonds will result in the overlap of the conduction band of titanium in TiO_2 and the d orbital of these dopant species to form new states lying just above the valence band. The band gaps of these samples calculated by the absorption edge are estimated to be 2.88–2.95 eV, which are much lower than those of P25 (~3.15 eV) and the nondoped anatase (3.2–3.3 eV). Also from the PLS and XPS results that many oxygen vacancies and Ti^{3+} species were produced from the doping of tungsten species. Thus the optical properties of the calcined material are also attributable to Ti^{3+} species and oxygen vacancies, as these have been reported to have transitions between 3.20 and 2.32 eV and are located above the valence band. The success in nitrogen and tungsten codoping and the increased photocatalytic activity of W,N-TiO_2 in the visible lights are observed in the present work. The closing of valence band and conduction band will undoubtedly improve the photocatalytic activity in the visible light region, which can be supported by results from UV–vis DRS and PLS spectra (Figs. 6 and 7).

On the other hand, it was widely reported that metal ion-doped TiO_2 will decrease the recombination rate of excited electron and holes. Puddu and co-workers had recently reported that the doped tungsten ions with high positive valence in W,N-TiO_2 will play as an electron acceptor and give favor to separate photo-excited electron/hole pairs. The W,N-TiO_2 catalysts show more photo-induced holes in the catalysts and lower recombination rate than the pure P25 as discussed in the UV–vis DRS section. Also from the XPS results, the W(VI) species in our present W,N-TiO_2 catalysts are considered to act as trapping site by accepting the photo-excited electrons from the TiO_2 valence band, and then generating W(V). In brief, these two processes cooperated to improve the efficiency of adsorbing visible light and form photo-induced electron and holes, which both enhance the W,N-TiO_2 photocatalytic activity under the visible light.

The purpose of Scheme 1 is to compare the band gap energy of TiO_2 and W,N-TiO_2. Scheme 1 gives a schematic mechanism diagram of these two processes. Pure TiO_2 with 3.2 eV banding energy irradiated by visible light cannot effectively produce enough photo-induced electrons and holes, which are considered to play an essential role in the photodegradation reactions. While the tungsten and nitrogen codoped TiO_2 will form new states just above the valence band. The band gap between the new states and the conduction band is about 2.9 eV, and thus the catalysts will be excited easily by visible light to produce the photo-induced electrons. Meanwhile, the doped W(VI) ions in the conduction band can capture the produced electrons to form W(V). The formed W(V) then can transfer the electrons to surface reducible species to improve the photocatalytic activity. These processes promote the separation of the photo-generated electrons and holes to accelerate the transmission of photocurrent carriers.

4. Conclusions

Tungsten and nitrogen codoped TiO_2 nano-photocatalysts with twist-like helix structure were prepared with a facile and template-free one-pot method, which showed higher visible light response compared with pure TiO_2 and P25. The W,N-TiO_2 samples were synthesized by simple hydrolysis of titania tetrachloride using ammonium tungstate as tungsten and nitrogen source. The novel photocatalysts showed both high ultraviolet and visible light photocatalytic activity in degrading phenol, while the 1%-W,N-TiO_2 sample gave the best photocatalytic activity and demonstrated to be far superior to that of the commercial Degussa P25 counterpart. The probable mechanism of codoping effect was proposed. The doped tungsten and nitrogen species can play a key role in narrowing the band gap and then in expanding the photoactivity to visible light region, also in decreasing the recombination rate of excited electron and holes. The high photoactivity of the W,N-codoped TiO_2 can also be attributed to the results of the synergetic effects of its high surface area, large pore volume, mesoporous pores, well-crystallized anatase special helix structure with regular holes on the wall.

Acknowledgements

We are grateful to the financial supports from the Major State Basic Resource Development Program (Grant no. 2003CB615807), NSFC (Project 20573024, 20407006), and the Natural Science Foundation of Shanghai Science & Technology Committee (06JC14004).

References

[1] L. Linsebigler, G.Q. Lu, J.T. Yates, Chem. Rev. 95 (1995) 735–758.
[2] T.N. Fujishima, D.A. Rao, J. Photochem. Photobiol. C 1 (2000) 1–21.
[3] D.W. Kormann, M. Bahnemann, R. Hoffmann, J. Phys. Chem. 92 (1988) 5196–5201.
[4] S. Klosek, D. Raftery, J. Phys. Chem. B 105 (2001) 2815–2819.
[5] S. Quadawi, S.R. Salman, J. Photochem. Photobiol. A 48 (2002) 161–169.
[6] S. Sato, Chem. Phys. Lett. 123 (1986) 126–128.
[7] R. Asahi, T. Morikawa, T. Ohwaki, K. Aoki, Y. Taga, Science 293 (2001) 269–271.
[8] J. Ovenstone, J. Mater. Sci. 36 (2001) 1325–1330.
[9] J. Moon, H. Takagi, Y. Fujishiro, M. Awano, J. Mater. Sci. 36 (2001) 949–956.
[10] J.C. Yu, J.G. Yu, W.K. Ho, Z.T. Jiang, L.Z. Zhang, Chem. Mater. 14 (2002) 3808–3816.
[11] V. Puddu, R. Mokaya, G.L. Puma, Chem. Commun. 45 (2007) 4749–4756.
[12] G. Marci, L. Palmisano, A. Sclafani, A.M. Venezia, R. Campostrini, G. Carturan, C. Martin, V. Rives, G. Solana, J. Chem. Soc. Faraday Trans. 92 (1996) 819–821.
[13] V. Keller, P. Bernhardt, F. Garin, J. Catal. 215 (2003) 219–222.
[14] Y.T. Kwon, K.Y. Song, W.L. Lee, G.J. Choi, Y.R. Do, J. Catal. 191 (2000) 192–199.
[15] M. Miyauchi, A. Nakajima, K. Hashimoto, T. Watanabe, Adv. Mater. 12 (2000) 1923–1927.
[16] H. Tade, A. Kokubu, M. Iwasaki, S. Ito, Langmuir 20 (2004) 4665–4670.
[17] B. Gao, Y. Ma, Y. Cao, W. Yang, J. Yao, J. Phys. Chem. B 110 (2006) 14391–14397.
[18] J.H. Xu, W.L. Dai, J.X. Li, Y. Cao, H.X. Li, K.N. Fan, Catal. Commun. 9 (2008) 246–249.
[19] J.H. Xu, J.X. Li, W.L. Dai, Y. Cao, H.X. Li, K.N. Fan, Appl. Catal. B 79 (2008) 72–80.
[20] K.Y. Song, M.K. Park, Y.T. Kwon, H.W. Lee, W.J. Chung, W.I. Lee, Chem. Mater. 13 (2001) 2349–2355.
[21] O. Carp, C.L. Huisman, A. Reller, Prog. Solid State Chem. 32 (2004) 33–177.
[22] G.V. Vasilenko, V.I. Zarembo, A. Slobodov, A. Russ, J. Appl. Chem. 70 (1997) 1498–1502.
[23] M.R. Hoffmann, S.T. Martin, W.Y. Choi, D.W. Bahnemann, Chem. Rev. 95 (1995) 69–96.
[24] J. Livage, Mater. Res. Soc. Symp. Proc. 73 (1986) 717.
[25] S. Doeuff, M. Henry, C. Sanchez, J. Livage, J. Non-Cryst. Solids 89 (1987) 206.
[26] M.T. Tsai, J. Non-Cryst. Solids 298 (2002) 116–130.
[27] Y. Wang, B. Wu, Q. Xu, Appl. Catal. B 59 (2005) 139–146.
[28] J.C. Yu, G.S. Li, X.C. Wang, X.L. Hu, C.W. Leung, Z.D. Zhang, Chem. Commun. 25 (2006) 2717–2719.
[29] H.X. Li, J.X. Li, Y.I. Huo, J. Phys. Chem. B 110 (2006) 1559–1565.
[30] H. Irie, Y. Watanabe, K. Hashmoto, J. Phys. Chem. B 107 (2004) 5483–5486.
[31] C.D. Wagner, W.M. Riggs, L.E. Davis, J.F. Moudler, G.E. Muilenberg (Eds.), Handbook of X-Ray Photoelectron Spectroscopy, PerkinElmer, 1992, p. 73.
[32] J. Pouilleau, D. Devilliers, H. Groult, J. Mater. Sci. 32 (1997) 5645–5650.
[33] K.E. Smith, V.E. Henrich, Phys. Rev. B 38 (1988) 5965–5969.
[34] H. Liu, W. Yang, Y. Ma, J. Yao, Appl. Catal. A 299 (2006) 218–226.
[35] J.L. Gole, J.D. Stout, C. Burda, Y.B. Lou, X.B. Chen, J. Phys. Chem. B 108 (2004) 1230–1240.
[36] S. Doniach, M. Sunjic, J. Phys. C 3 (1970) 285–289.
[37] F. Le Normand, J. El Fallah, L. Hilaire, P. Lègarè, A. Kotanj, J.C. Parlebas, Solid State Commun. 71 (1989) 885–889.
[38] M. Valigi, D. Gazzoli, I. Pettit, G. Mattei, S. Colonna, S. DeRossi, G. Ferraris, Appl. Catal. A: Gen. 231 (2002) 159–172.
[39] F.B. Li, X.Z. Li, Chemosphere 48 (2002) 1103–1111.
[40] J. Zhang, Y. Hu, M. Matsuoka, H. Yamashita, M. Minagawa, H. Hidaka, J. Phys. Chem. B 105 (2001) 8395–8398.
[41] Y. Cong, J. Zhang, F. Chen, M. Anpo, D. He, J. Phys. Chem. C 111 (2007) 10618–10623.
[42] H. Yamashita, Y. Ichihashi, M. Anpo, J. Phys. Chem. 100 (1996) 16041–16044.